BUCKLING OF LAMINATED-GLASS BEAMS USING THE EFFECTIVE-THICKNESS CONCEPT

M López-Aenlle[a*], F. Pelayo[a], G. Ismael[a], M. G. Prieto[a], A. Martín[a], A. Fernández-Canteli[a].

[a]Department of Construction and Manufacturing Engineering, University of Oviedo, Campus de Gijón, Zona Oeste, Edificio 7, 33203, Gijón, Spain.

[*]corresponding author; E-mail: aenlle@uniovi.es
Phone: +34985 182057, Fax: +34985 18 2433

ABSTRACT

Structural stability is one of the design requirements in laminated-glass beams and plates due their slenderness and brittleness. In this paper the equations of the classical Euler theory for buckling of isotropic monolithic beams are extended to laminated-glass beams using the effective thickness and the effective Young modulus concepts. It is demonstrated that the dependency of the effective stiffness on boundary conditions can be considered using buckling ratios of Euler theory corresponding to isotropic linear monolithic beams. The analytical predictions are validated by compressive experimental tests in simply supported beams. Fixed boundary conditions are difficult to reproduce in experimental tests due to the brittleness of the glass and for this reason fixed-fixed and fixed-pinned boundary conditions were validated using a finite element model.

KEYWORDS

Laminated glass, structural composites, PVB, bucking, structural stability, viscoelasticity.

NOMENCLATURE

E_{eff} Effective Young modulus

E Glass Young modulus of glass layers

$E_2(t)$ Viscoelastic relaxation tensile modulus for polymeric interlayer

$G_2(t)$ Viscoelastic relaxation shear modulus for the polymeric interlayer

H_1 Thickness of glass layer 1 in laminated glass

H_2 Thickness of polymeric layer 2 in laminated glass

H_3 Thickness of glass layer 3 in laminated glass

$H_{TOT} = H_1 + H_2 + H_3$

$H_0 = H_2 + \left(\frac{H_1 + H_3}{2}\right)$

I Second moment of area

$I_1 = \frac{H_1^3}{12}$

$I_3 = \frac{H_3^3}{12}$

$I_T = I_1 + I_3 = \frac{H_1^3 + H_3^3}{12}$

$I_{TOT=} = I_T(1 + Y)$

$K_2(t, T)$ Viscoelastic bulk modulus

L Length of a glass beam

$P(t, T)$ Critical load

T	Temperature
T_0	Reference temperature

$$Y = \frac{H_0^2 H_1}{I_T(H_1+H_3)}$$

LOWERCASE LETTERS

a_T	Shift factor
b	Width of a glass beam
$g(x)$	Shape function (Galuppi and Royer Carfagni model)
t	Time
w	Deflection

GREEK LETTERS

η_2	Loss factor of the polymeric interlayer of laminated glass
ν_1	Poisson ratio of the glass layers
$\nu_2(t,T)$	Viscoelastic Poisson ratio of the polymeric interlayer

1 INTRODUCTION

Laminated glass is a sandwich or layered material which consists of two or more plies of monolithic glass with one or more interlayers of a polymeric material with mechanical properties that are time (or frequency) and temperature dependent [1]. Polyvinyl butyral (PVB) is the most widely used interlayer material, although the new ionoplastic interlayers improve the mechanical properties of laminated glass for a broad range of temperatures [1]. Polyvinyl butyral (PVB) is sold in thicknesses of 0.38 mm or a multiple of this value (0.76 mm, 1.12 mm, and 1.52 mm).

Laminated glass is easy to assemble in a finite element model but many small 3D elements are needed to mesh accurately because the thickness of the viscoelastic interlayer is usually very small compared with the dimension of the laminated-glass element. Cubic elements in 3D and square elements in 2D generally result in equations that are well conditioned but if the element shape is greatly distorted from these ideal shapes, numerical difficulties can arise [2]. If we wish to mesh the interlayer of a square laminated-glass plate $2000\ mm \times 2000\ mm$ with 2 cubic elements along the thickness, we would need approximately 27.7×10^6 elements only to mesh the interlayer. Moreover, if a quasi-static analysis is performed taking into account the temperature and time-dependent behaviour of the interlayer, the time needed to perform the calculation is considerably higher than that needed for a static analysis. Consequently, the 3D models in laminated-glass elements are very costly in time and memory.

The calculation of laminated-glass elements can be facilitated by simplifying the viscoelastic solution using the quasi-elastic method, which consists of describing the viscoelastic behaviour of the interlayer by an elastic behaviour with parameters that depend on the load duration and temperature [3, 4, 5, 6, 7]. This means that the memory effect of the viscoelastic material is neglected and that the mechanical properties are linear elastic but time dependent [7, 8, 9].

The concept of effective thickness has been proposed in recent years [7, 9, 10] based on the quasi-elastic solution. This method consists of calculating the thickness (time and temperature dependent) of a monolithic element with bending properties equivalent to those of the laminated one, that is, the deflections provided by the equivalent monolithic beam are equal to those of the layered model with a viscoelastic core. The effective

thickness can then be used in analytical equations and simplified finite element models in place of the layered laminated-glass element [7, 9, 10, 11]. The effective-thickness concept is proposed in most of the technical standards related to laminated glass and it is more readily applicable in design practice. The effective-thickness concept is not easy to implement in finite element programs because a monolithic model with constant Young modulus and a temperature- and time-dependent thickness has to be defined. As the effective thickness is derived from the effective stiffness [7, 9, 10], an effective Young modulus [11] can also be inferred from the effective stiffness, this being more attractive to be used in numerical models (a monolithic model with constant thickness is defined whereas the Young modulus is time and temperature dependent). Thus, the effective-thickness and the effective Young modulus concepts can be used interchangeably with the same accuracy.

The effective-thickness concept allows also stress-effective thickness to be defined, i.e. the thickness of a monolithic beam with equivalent bending properties in terms of stresses. However, due to the fact that the buckling behaviour is governed by its flexural stiffness, only the deflection effective thickness is considered in this paper.

If laminated-glass elements are subject to compressive loads, structural stability is one of the design requirements because laminated-glass elements are brittle and slender. Due to the fact that the stiffness of the interlayer is temperature and time dependent, the same is true of the critical load, that is, the critical load of a laminated-glass beam subject to constant compressive load decreases with time.

Several analytical models have been proposed for determining the critical load of a simply supported laminated-glass beam [12, 13, 14, 15] but only a few are devoted to other boundary conditions [16]. In monolithic beams, the effect of the boundary conditions is considered through the buckling ratio β (or alternatively with the effective length L_{eff}) whereas the stiffness EI is constant. In this paper, we demonstrate that the effective stiffness also depends on the boundary conditions and its effect can also be taken into account through the buckling ratio β.

The aim of this paper is to propose a simplified method to calculate critical loads in laminated-glass beams with different boundary conditions using the Euler theory [17] of monolithic beams, the quasi-elastic solution [8, 9] and the effective-stiffness concept [7,

8, 9, 10]. As a means of validating the model, the critical load of several laminated-glass beams, made of annealed glass plies and a PVB core, were predicted using the effective stiffness concept and validated by experimental tests and numerical models.

1.1 The effective-thickness concept

The concept of effective thickness for calculating deflections in laminated-glass beams under static loads was proposed by Calderone et al. [7] based on a previous work of Wölfel [18]. Later, Galuppi and Royer-Carfagni [9] derived new equations for the deflection effective thickness using a variational approach and assuming that the deflection shape of the laminated-glass beam coincides with that of a monolithic beam under the same load and boundary conditions; that is, the deflection of the beam is assumed to be:

$$w(x,t,T) = -\frac{g(x)}{EI(t,T)_S} \tag{1}$$

where g(x) is a shape function that takes the form of the elastic deflection of a monolithic beam with constant cross section under the same load and boundary conditions as the laminated-glass beam and where $EI(t)_S$ is the bending stiffness of the laminated-glass beam given by:

$$EI(t,T)_S = \frac{1}{\frac{\eta_S(t,T)}{EI_T(1+Y)} + \frac{1-\eta_S(t,T)}{EI_T}} \tag{2}$$

Where:

$$\eta_S(t,T) = \frac{1}{1+\frac{EH_1H_2H_3\psi_B}{(1+Y)G_2(t,T)(H_1+H_3)}} \tag{3}$$

The parameter ψ_B [9] can be expressed as:

$$\psi_B = \frac{\gamma}{L^2} \tag{4}$$

with γ being a constant parameter which depends on the boundary and load conditions [9].

Calderone et al. [7] proposed an effective stiffness for a laminated-glass beam subjected to static loads, which is expressed as:

$$EI(t,T)_S = EI_T\ (1 + \Gamma_S(t)Y) \tag{5}$$

where

$$\Gamma_S(t,T) = \frac{1}{1 + 9.6\dfrac{E\ H_1\ H_2\ H_3}{G_2(t,T)\ (H_1 + H_3)\ L^2}} \tag{6}$$

Eqs. (2) and (5) can be expressed in a unified form as

$$EI(t,T)_S = EI_T \left(1 + \frac{Y}{1 + \gamma\dfrac{E\ H_1\ H_2 H_3}{G_2(t,T)\ (H_1 + H_3)\ L^2}} \right) \tag{7}$$

Eq. (6) proposed by Calderone et al. [7] is based on a previous work of Wölfel devoted to composite sandwich structures under various boundary and loading conditions, leading to different values of the parameter γ. Calderone et al. [7] proposed $\gamma = 9.6$ for all the boundary conditions, although in Wölfel's formulation [18] this is associated with a simply supported beam under uniformly distributed load.

Galuppi and Royer Carfagni [9] proposed to calculate the parameter ψ_B by means of:

$$\psi_B = \frac{\int_0^L g''(x)^2 dx}{\int_0^L g'(x)^2 dx} \;\; ; \qquad 0 \le x \le L \tag{8}$$

The authors derived $\psi_B = 10/\mathrm{L}^2$ for a beam under concentrated load and $\psi_B = \frac{168}{17L^2} = \frac{9.882}{L^2}$ for a beam under distributed load. Assuming a bending deflection sinusoidal in shape (equivalent to consider a sinusoidal load) given by:

$$g(x) = sin\left(\frac{\pi x}{L}\right) \;\; ; \qquad 0 \le \mathrm{x} \le \mathrm{L} \tag{9}$$

it is derived that $\psi_B = \frac{\pi^2}{L^2}$

Parameter Y in Eqs. (4) and (7) is a constant coefficient that relates the monolithic and the layered limits of the effective stiffness $EI(t,T)_S$ by means of the expression

$$1 + Y = \frac{monolithic\ limit\ of\ EI(t,T)_S}{layered\ limit\ of\ EI(t,T)_S} = \frac{EI(0,T)_S}{EI(\infty,T)_S} \tag{10}$$

Thus, the layered limit is given by EI_T and the monolithic limit by $EI_T(1+Y)$, respectively.

1.2 Analytical models for the buckling strength of laminated-glass columns

Foraboschi [19] developed a mathematical model for determining the critical load, on laminated-glass columns subjected to compressive loads and provides a closed-form expression to calculate the critical load, which is expressed as:

$$\frac{P_{crit}(\mathrm{t,T})}{b} = \frac{EH^3}{2L^2} + \frac{2HG_2(t,T)}{H_2}\int_0^L \xi'(x)dx \tag{11}$$

where $\xi(x)$ is a function that describes the axial relative translation of the inner edge of the glass ply with respect to the axial axis.

The model is derived for a cantilever beam but the author proposes to extend the technique to other boundary conditions using an effective length. A sensitivity analysis shows that buckling strength depends on the thickness of the core, the environmental temperature, and the load duration. The paper also provides rules in order to use laminated glass for compressive elements.

Blaauwendraad [12] proposed a formula for the buckling force of a simply supported laminated-glass column which is expressed as:

$$\frac{P_{crit}(\mathrm{t,T})}{b} = \frac{\pi^2 E I_T}{L^2} + \frac{H_0^2}{\frac{L^2}{\pi^2 E H_1} + \frac{L^2}{\pi^2 E H_3} + \frac{H_2}{G_2(t,T)}} \tag{12}$$

The layered and the monolithic limits are easy to calculate considering $G_2(t,T) = 0$ and $G_2(t,T) = \infty$, respectively. As pointed out by the author, this equation coincides with the equation derived by Satler and Stein [13] for sandwich panels.

Aiello et al. [20] performed some experimental compressive tests on glass panels and columns. These authors concluded that the buckling strength of the panels depends greatly on their slenderness and that the model of Blaauwendraad [12] provides a good approximation of the buckling force.

Feldmann et al. [15] proposed to calculate the critical load of a simply supported beam with the Euler Theory but using effective stiffness, i.e.:

$$\frac{P_{crit}(\mathrm{t,T})}{b} = \frac{\pi^2 E I_{eff}}{L^2} \tag{13}$$

where

$$EI_{eff} = EI_T \left(1 + \frac{Y}{1 + \frac{E\, H_1\, H_2\, H_3}{G_2(t,T)\,(H_1 + H_3)} \frac{\pi^2}{L^2}} \right) \tag{14}$$

Galuppi and Royer-Carfagni [14] developed an analytical model for the buckling of a simply supported laminated-glass column with viscoelastic core under a compressive load

$P(t)$ which can be time dependent. A full viscoelastic solution is developed, although it is complex because the classical superposition of solutions commonly used in linear viscoelasticity through Bolztman integral cannot be used due to the geometric nonlinearities associated with the buckling phenomenon [14].

A simpler model was derived using the quasi-elastic approximation which neglects the memory effect [14]. Assuming that the beam axis presents an initial sinusoidal imperfection given by:

$$w_o(x,t) = e\,sin\left(\frac{\pi x}{L}\right) \tag{15}$$

and considering the deflection of the beam (figure 1) as:

$$w(x,t,T) = a(t,T)\,sin\left(\frac{\pi x}{L}\right) \tag{16}$$

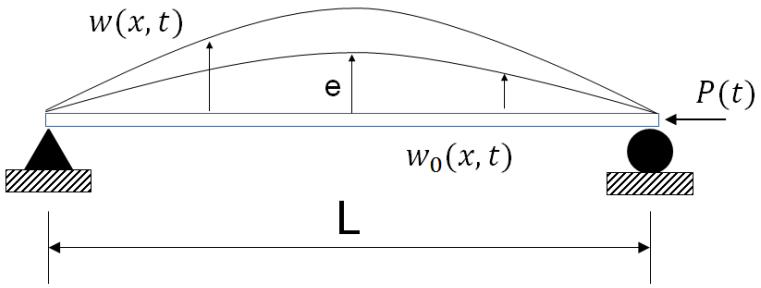

Figure 1. Schematic representation of a simply supported beam with an initial deformation.

the authors derived a simple equation for the critical load of a simply supported beam, which is given by the equation:

$$\frac{P_{crit}(t,T)}{b} = \frac{\pi^2}{L^2} EI_T \left(\frac{G_2(t,T)\cdot \frac{I_{TOT}}{I_T} L^2 + \frac{EH_1H_3H_2\pi^2}{(H_1+H_3)}}{G_2(t,T)\cdot L^2 + \frac{EH_1H_3H_2\pi^2}{(H_1+H_3)}} \right) \tag{17}$$

Eq. (14) can also be expressed as:

$$\frac{P_{crit}(t,T)}{b} = \frac{\pi^2}{L^2} EI_T \left(1 + \frac{Y}{1 + \frac{EH_1H_2H_3}{G_2(t,T)(H_1+H_3)} \frac{\pi^2}{L^2}} \right) \tag{18}$$

After simple manipulations, it can be easily demonstrated that the Eq. (18) derived by Galuppi and Royer Cargfagni [14] for a simply supported beam coincides with that [Eq. (12)] developed by Blaauwendraad [12] and with that [Eq. (13)] derived by Feldman et al. [15].

The time-dependent deflection $a(t,T)$ of the beam is given by:

$$a(t,T) = \frac{\left(\frac{\mathrm{G}_2(t,T)(H_1+H_3)}{H_2EH_1H_3} + \frac{\pi^2}{L^2} \right) P(t)e}{EI_T \frac{\pi^4}{L^4} - \frac{\pi^2}{L^2} \mathrm{P}(t) + \frac{\mathrm{G}_2(t,T)(H_1+H_3)}{H_2H_1H_3} \left(\frac{\pi^2}{L^2} I_{TOT} - \frac{P(t)}{E} \right)} \tag{19}$$

which can also be expressed as:

$$a(t,T) = \frac{\left(\frac{\mathrm{G}_2(t,T)(H_1+H_3)}{H_2EH_1H_3} + \frac{\pi^2}{L^2} \right) P(t)e}{EI_T \frac{\pi^2}{L^2} \left(\frac{\pi^2}{L^2} + \frac{\mathrm{G}_2(t,T)(H_1+H_3)}{EH_2H_1H_3}(1+Y) \right) - \mathrm{P(t)} \left(\frac{\pi^2}{L^2} + \frac{\mathrm{G}_2(t,T)(H_1+H_3)}{EH_2H_1H_3} \right)} \tag{20}$$

Amadio and Bedon [21] developed an analytical model for the buckling of laminated-glass beams based on the Euler theory and the effective stiffness $EI(t,T)_s$ proposed by Calderone et al. [8], i.e.:

$$\frac{P_{crit}(\mathrm{t,T})}{b} = \frac{\pi^2 EI(t,T)_s}{L^2} \tag{21}$$

where $EI(t,T)_s$ is given by Eq. (5). The authors observed that the Eq. (21) overestimates the critical load when using the parameter $\Gamma_S(t,T)$ given by Eq. (6) and they suggest modifying this equation by introducing a new parameter δ as:

$$\Gamma_S(t,T) = \frac{1}{1 + 9.6\delta \frac{E\ H_1\ H_2\ H_3}{G_2(t,T)\ (H_1+H_3)\ L^2}} \tag{22}$$

From numerical simulations, they arrived at $\delta = 1.03$ for a simply supported beam, i.e. $\gamma = 9.6 \cdot \delta = 9.888$. This value agrees well with Eq. (18), derived by Galuppi and Royer Carfagni [14], where $\gamma = \pi^2 = 9.870$.

1.3 On the layered and monolithic limits of laminated-glass beams

The works of Norville [22] and Galuppi and Royer-Carfagni [9] have pointed out that the response of laminated-glass beams presents two borderlines: 1) the layered limit corresponding to the case when the beam consists of free-sliding glass plies and 2) the monolithic limit, when the Euler–Bernoulli assumptions hold (plane sections remain plane) for the entire section of the laminated-glass element (the response of the composite beam approaches that of a homogeneous glass beam with inertia equal to the inertia of the properly spaced glass layers of the interlayer gaps) [9].

PVB mechanical behavior can be established by relaxation or creep tests in the time domain or its corresponding dynamic tests in the frequency domain [23]. The relaxation master curve of the shear modulus $G_2(t,T)$ at temperature T is usually fitted with a generalized Maxwell model which can be represented with a Prony series given by [24]:

$$G_2(t,T) = G_2^{\infty} + \sum_{i=1}^{n} g_i \, \mathrm{e}^{\left(-\frac{t}{\tau_i}\right)} = G_2^{0} - \sum_{i=1}^{n} g_i \, (1 - \mathrm{e}^{\left(-\frac{t}{\tau_i}\right)}) \qquad (23)$$

The shear modulus $\mathrm{G}_2(t,T)$ for the polyvinyl butyral [10] is presented in figure 2, which shows that the $\mathrm{G}_2(t,T)$ presents a minimum value $\mathrm{G}_2^{\infty} = \mathrm{G}_2(\infty,T)$ for the long term and a maximum value $\mathrm{G}_2^{0} = \mathrm{G}_2(0,T)$ for the short term. Thus, for laminated-glass beams, two different borderlines need to be defined: (1) the long-term limit associated with G_2^{∞} and (2) the short-term limit associated with G_2^{0} .

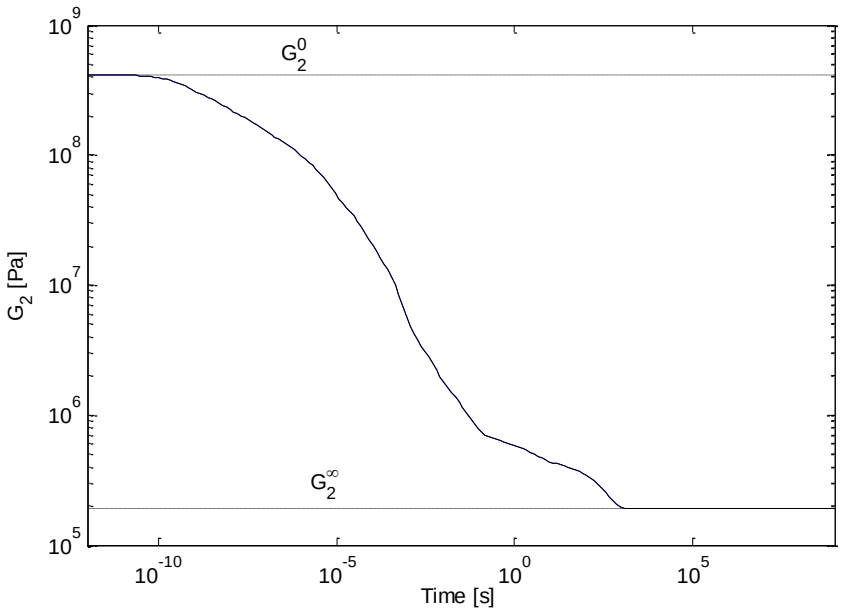

Figure 2. Shear-relaxation modulus for the PVB at $T = 20^o C$ [10].

The parameter $\eta_S(t)$ in Eq. (3) takes values in the range $0 \leq \eta_S(t) \leq 1$, $\eta_S = 0$ corresponding to the case of a layered beam and $\eta_S = 1$ to a monolithic beam. The layered limit is reached when the term:

$$\frac{E\ H_1\ H_2 H_3 \psi_B}{(1+Y)\ G_2(t,T)\ (H_1+H_3)} \tag{24}$$

in Eq. (3) is negligible with respect to one. $G_2(t,T)$ can take small values but not zero, meaning that the layered limit is never reached. However, we can be very close to the layered limit with short beams, boundary conditions related to high values of γ and low values of $G_2(t,T)$, i.e. for the long term. This effect is presented in figure 2, which shows the effective stiffness at $T = 20^o C$ of a simply supported short beam with $L = 0.2\ m$, and a longer beam with L =1.2 m, both having the following geometrical dimensions and mechanical properties: $b = 10\ cm$, $H_1 = H_3 = 3\ mm$, $H_2 = 0.38\ mm$, $E = 70E9\ Pa$ and $\nu = 0.2$.

The monolithic limit is reached when the term given by Eq. (24) tends to infinity. Again, this limit is never reached, but due to the relative high magnitude of ($G_2(t,T)$ over the short term, the monolithic limit is always very close to the maximum limit given by G_2^0.

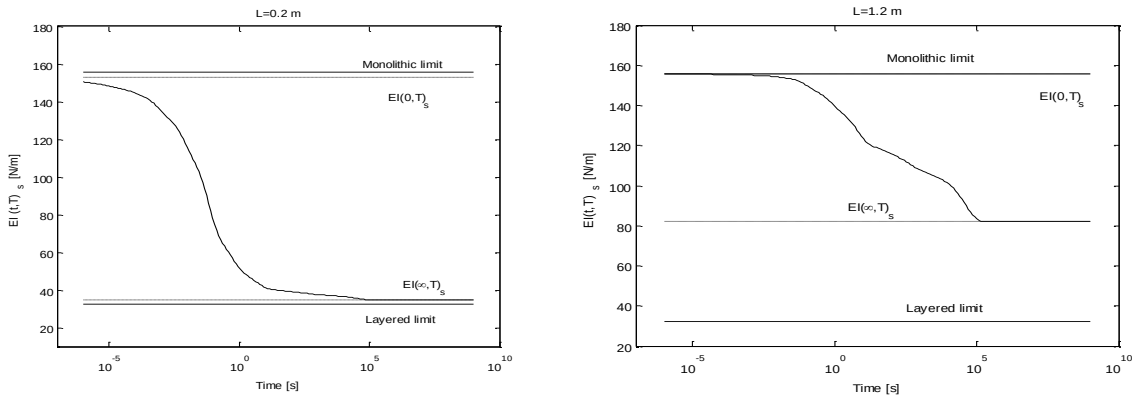

Figure 3. Effective stiffness of a simply supported beam with different lengths at $T = 20^{o}C$.

From Eq. (18), we infer that the maximum critical load occurs at $t = 0$; that is, it depends explicitly on the instantaneous shear modulus $\mathrm{G}_2^0 = \mathrm{G}_2(0,T)$ on the interlayer. The critical load corresponding to $\mathrm{G}_2^0 = \mathrm{G}_2(0,T)$ is hereafter referred to as $\mathrm{P}_{\mathrm{crit}}^0$ (glassy critical load in [14]). On the other hand, the minimum critical load, hereafter referred to as $\mathrm{P}_{\mathrm{crit}}^\infty$ (rubbery critical load in [14]), is reached at $t = \infty$ and it depends on the long-term shear modulus $\mathrm{G}_2^\infty = \mathrm{G}_2(\infty,T)$. Thus, using the quasi-elastic approximation, three different cases can be considered in the buckling of a laminated-glass beam subject to a constant compressive load P [14]:

1. $\mathrm{P} > \mathrm{P}_{\mathrm{crit}}^0$. In this case the load P is larger than that corresponding to the short-term limit ($\mathrm{G}_2(0,T) = \mathrm{G}_2^0$) and immediate buckling occurs at $t = 0$.
2. $\mathrm{P} < \mathrm{P}_{\mathrm{crit}}^\infty$. In this case the load P is less than that corresponding to the long-term limit ($\mathrm{G}_2(\infty,T) = \mathrm{G}_2^\infty$) and no buckling occurs at any time.
3. $\mathrm{P}_{\mathrm{crit}}^0 > \mathrm{P} > \mathrm{P}_{\mathrm{crit}}^\infty$. The buckling instability occurs at a certain critical time t_{crit}, which depends on the magnitude of the load P and on the temperature. This phenomenon is known as creep buckling [14].

In [14] it is demonstrated that the glassy critical load $\mathrm{P}_{\mathrm{crit}}^0$and the rubbery critical load $\mathrm{P}_{\mathrm{crit}}^\infty$ obtained with the quasi-elastic approximation coincide with those derived using the full viscoelastic analysis because the quasi-elastic and the viscoelastic solutions have the same behaviour at $t = 0$ and $t \to \infty$. The three aforementioned different cases are of theoretical interest, but for practical applications a safe procedure is needed in order to

avoid failures due to buckling, i.e. the compressive load acting of the beam must be less than P_{crit}^{∞} . Therefore, the quasi-elastic solution can be used advantageously to determine safe critical loads in laminated glass, avoiding the use of more complex models.

2 CRITICAL LOAD OF LAMINATED-GLASS BEAMS COMBINING THE EULER THEORY AND THE EFFECTIVE STIFFNESS

As illustrated in Section 1, most of the analytical models proposed for the buckling of laminated-glass beams are valid for simply supported beams. The effective thickness proposed by Galuppi and Royer Carfagni [9] and the effective stiffness proposed by Feldman et al. [15] use parameters which depend on the load and boundary conditions. The effective thickness [9] and the effective stiffness [15] can be extended to calculate the buckling of a simply supported beam, assuming a sinusoidal transversal load (equal in shape to the buckling deflection of a monolithic beam with the same boundary conditions).

In this section, a simple expression to calculate the buckling load of a laminated-glass beam with any kind of boundary condition is derived. The critical load of a linear-elastic monolithic beam, according to the Euler theory is given by [25]:

$$P_{crit} = \frac{\pi^2 E\, I}{(\beta L)^2} \tag{25}$$

where β is the buckling ratio. In the present paper, we propose extending the equations of the Euler Theory for monolithic beams to laminated-glass beams, substituting the stiffness EI in Eq. (25) by the effective stiffness $\mathrm{EI(t,T)_S}$ given by Eq. (7), i.e.:

$$P_{crit}(t,T) = \frac{\pi^2 EI(t,T)_S}{(\beta L)^2} \tag{26}$$

The critical load of an elastic monolithic beam with constant cross section and stiffness EI, using the Rayleigh Ritz method [25] with an approximate deflection curve $g(x)$, is given by:

$$P_{crit} = \frac{\pi^2 EI}{\left(L_{eff}\right)^2} = \frac{\int_0^L EIg''(x)^2 dx}{\int_0^L g'(x)^2 dx} \tag{27}$$

where L_{eff} is the effective length. Identifying Eqs (8) and (27) gives:

$$L_{eff} = \frac{\pi}{\sqrt{\psi_B}} \tag{28}$$

This means that the parameter ψ_B is related to the buckling ratio β by means of the equation:

$$\psi_B = \frac{\pi^2}{L_{eff}^2} = \frac{\pi^2}{\beta^2 L^2} \tag{29}$$

For a simply supported beam, $\beta = 1$ and the Eq. (29) coincides with the results provided by Eq. (8) using a sinusoidal shape for $g(x)$. If Eq. (29) is substituted in Eq. (3), it becomes:

$$\eta_S(t,T) = \frac{1}{1 + \frac{E_1 H_1 H_2 E_3 H_3}{(1+\mathrm{Y})\mathrm{G}_2(t,T)(E_1 H_1 + E_3 H_3)} \frac{\pi^2}{\beta^2 L^2}} \tag{30}$$

The effective stiffness given by Eq. (7) can be expressed as:

$$EI(t,T)_S = EI_T \left(1 + \frac{Y}{1 + \frac{E_1 H_1 H_2 E_3 H_3}{G_2(t,T)(E_1 H_1 + E_3 H_3)} \frac{\pi^2}{(\beta L)^2}} \right) \tag{31}$$

It can be seen in Eq. (31) that the effective stiffness depends on the boundary conditions through the buckling ratio β. This means that the concept of effective buckling length used in monolithic beams with the Euler theory cannot be directly extended to laminated-glass beams, that is, the critical loads are not proportional to $\left(\frac{1}{\beta}\right)^2$.

If Eq. (31) is substituted in Eq. (26), the latter becomes:

$$P_{crit}(t,T) = \frac{\pi^2}{(\beta L)^2} EI_T \left(1 + \frac{Y}{1 + \frac{E_1 H_1 H_2 E_3 H_3}{G_2(t,T)(E_1 H_1 + E_3 H_3)} \frac{\pi^2}{(\beta L)^2}} \right) \tag{32}$$

Eq. (32), a general equation to calculate the critical load of a laminated-glass beam under compressive loads, presents the following advantages:

- It is easy to use.
- It is a general formula which can be applied to any kind of boundary conditions.
- The buckling ratios of the Euler Theory for monolithic beams can be used for laminated-glass beams.

For a simply supported beam the bucking ratio is $\beta = 1$ and Eq. (32) can be expressed as:

$$P_{crit}(t,T) = \frac{\pi^2}{L^2} EI_T \left(\frac{G_2(t,T) \cdot \frac{I_{TOT}}{I_T} \cdot L^2 + \frac{EH_1H_2H_3\pi^2}{(H_1+H_3)}}{G_2(t,T) \cdot L^2 + \frac{EH_1H_2H_3\pi^2}{(H_1+H_3)}} \right) \quad (33)$$

Which coincides with the quasi-elastic solution derived by Blaauwendraad [12], Galuppi and Royer Carfagni [14] and Feldman et al. [15] for a simply supported laminated-glass beam.

With respect to the bending deflection of a simply supported laminated-glass beam under a compressive load $P(t)$, if Eq.(33) is substituted in Eq.(19), the latter can be expressed as:

$$a(t,T) = \frac{eP(t)}{P_{crit}(t,T) - P(t)} \quad (34)$$

If buckling is defined as the load corresponding to $a(t,T) \to \infty$ [14], from Eq. (34) it is inferred that buckling will occur when:

$$P_{crit}(t,T) = P(t) \quad (35)$$

i.e. when the curves corresponding to $P(t)$ and $P_{crit}(t,T)$ intersect (see figure 4). The time at which $a(t,T) \to \infty$ (intersection of $P(t)$ and $P_{crit}(t,T)$) is hereafter referred to as critical time t_{crit} whereas the buckling load [load corresponding to the intersection of $P(t)$ and $P_{crit}(t,TP_{crit}(t,T)$] is referred to as N_{crit}.

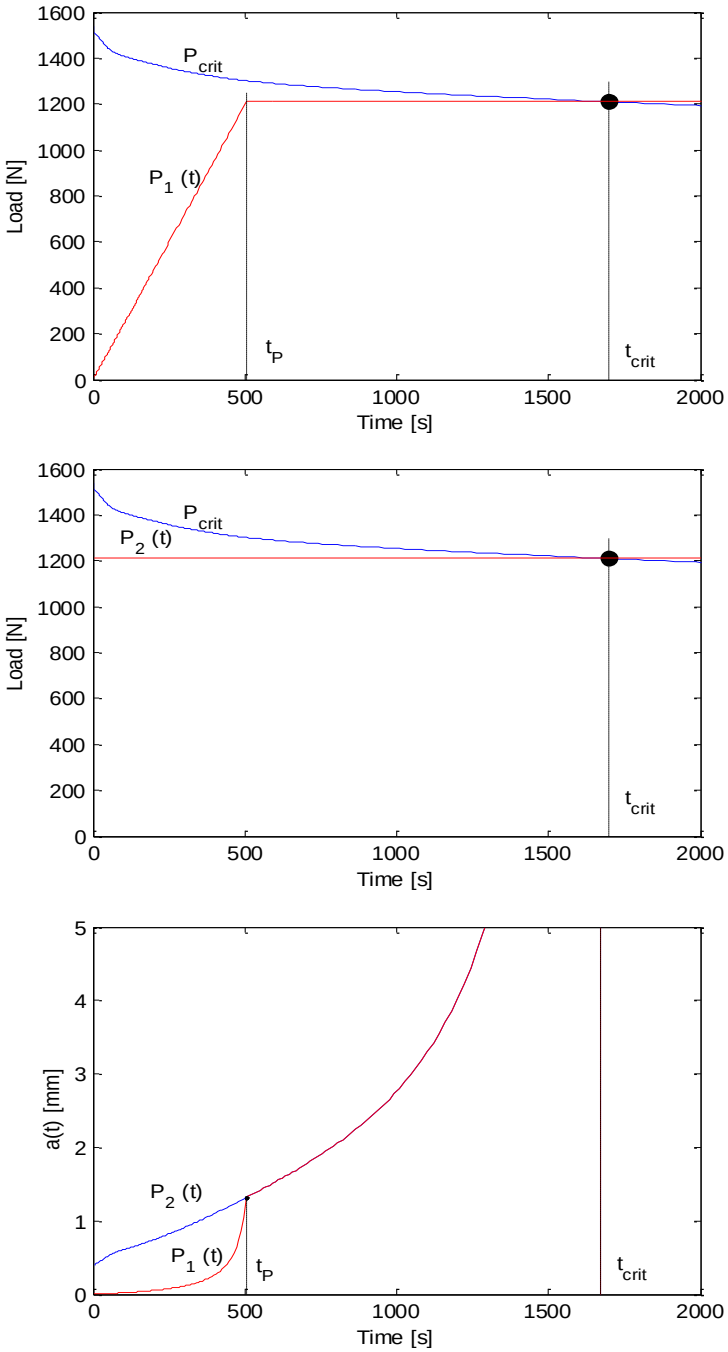

Figure 4. Buckling of a laminated-glass beam using the quasi-elastic approximation a) non-constant axial load P1(t); b) constant axial load P2(t); c) bending deflection a(t) for both loads, P1(t) and P2(t).

As the solution is elastic the two load histories $P_1(t)$ and $P_2(t)$ shown in figure 4 present the same buckling critical load N_{crit} and the same critical time t_{crit}; that is, the load history at short times ($t < t_{crit}$) does not influence the prediction of the buckling

phenomenon with the quasi-elastic solution. This is important in practical terms because it is not possible to perform buckling experiments subjecting the laminated-glass beam to a constant load, since $t = 0$. In this paper, the load histories presented in figures 5, 6, 8, 10 and 11 were used in the experiments.

According to the Euler theory, the bending deflection of an elastic monolithic beam [25] is given by:

$$w = a\,sin\left(\frac{\pi x}{L}\right) \tag{36}$$

where

$$a = \frac{eP}{\frac{\pi^2 EI}{L^2} - P} \tag{37}$$

If the stiffness EI in Eq. (34) is substituted by the effective stiffness $EI(t,T)_s$ and the load P by $P(t)$, Eq. (34) results in:

$$a(t,T) = \frac{\left(\frac{G_2(t,T)(H_1+H_3)}{H_2 E H_1 H_3} + \frac{\pi^2}{L^2}\right) P(t) e}{\left(EI_T \frac{\pi^2}{L^2} - P(t)\right)\left(\frac{\pi^2}{L^2} + \frac{G_2(t,T)(H_1+H_3)}{E H_2 H_1 H_3}\right) + (1+Y)\frac{G_2(t,T)(H_1+H_3)}{E H_2 H_1 H_3}} \tag{38}$$

This coincides again with the solution derived by Galuppi and Royer Carfagni using the quasi-elastic solution [14], demonstrating that the equations of the Euler Theory for elastic monolithic beams can be easily extended to laminated-glass beams (with the quasi-elastic approximation) using the effective stiffness or the effective thickness.

2.1 Methodology

If the buckling ratio of a monolithic beam with the same boundary conditions as the laminated glass one is known from the literature, the technique consists of calculating the buckling load using Eq. (32).

An alternative consists of using the Euler Theory to calculate the critical load $P_{crit-MON}$ of a monolithic beam with the same boundary conditions and thickness H_{TOT}, and then calculate the critical load $P_{crit-LG}$ of the laminated glass one by means of:

$$P_{crit-LG}(t,T) = P_{crit-MON}\frac{EI(t,T)_S}{E\frac{H_{TOT}^3}{12}} \tag{39}$$

On the contrary, if the buckling ratio is not known from the literature, the following procedure can be followed:

1) A finite-element monolithic model with thickness H_{TOT}, length L and Young modulus E have to be assembled. The buckling ratio β can be calculated from:

$$P_{crit-MON} = \frac{\pi^2 E\ bH_{TOT}^3}{12(\beta L)^2} \tag{40}$$

where $P_{crit-MON}$ is the critical load calculated with the monolithic FE model.

2) To calculate the Buckling load with expression (32) or expression (39).

2.2 Using Monolithic Models

In recent papers, the effective-thickness concept [7, 9, 10, 11] has been proposed to calculate deflections and stresses in laminated-glass beams using the quasi-elastic approximation. This means that a thickness dependent on temperature and load duration has to be defined. The effective Young modulus is more appealing for use in numerical models because a monolithic beam with constant thickness can be assembled in the FE program whereas the material is defined as time and temperature dependent using the effective Young modulus. An effective Young modulus to be used with constant cross sections of monolithic models can be derived from:

$$\frac{E_{eff}(t,T)H_{TOT}^3}{12} = EI(t,T)_S \tag{41}$$

from which it is inferred that [11]:

$$E_{eff}(t,T) = E\frac{(H_1^3+H_3^3)}{H_{TOT}^3}\left(1+\frac{Y}{1+\frac{EH_1H_2H_3}{\mathrm{G}_2(t,T)(H_1+H_3)}\frac{\pi^2}{(\beta L)^2}}\right) \tag{42}$$

3 ANALYTICAL PREDICTIONS AND EXPERIMENTAL TESTS

A simply supported beam with the following geometrical data: $H_1 = 2.9$ mm, $H_3 = 2.9$ mm, $H_2 = 0.38$ mm, $L = 0.7$ m and $b = 0.1$ m was tested at temperature $T = 24^o C$ in a 250 kN axial machine (MTS810) (see figure 5). The axial displacement of the beam was increased with a constant rate of 0.01 mm/min. The relation between the axial force recorded by the machine and the bending deflection at the mid-span measured with a laser sensor, is presented in figure 5. The test was stopped when the bending deflection reached the magnitude of 7 mm.

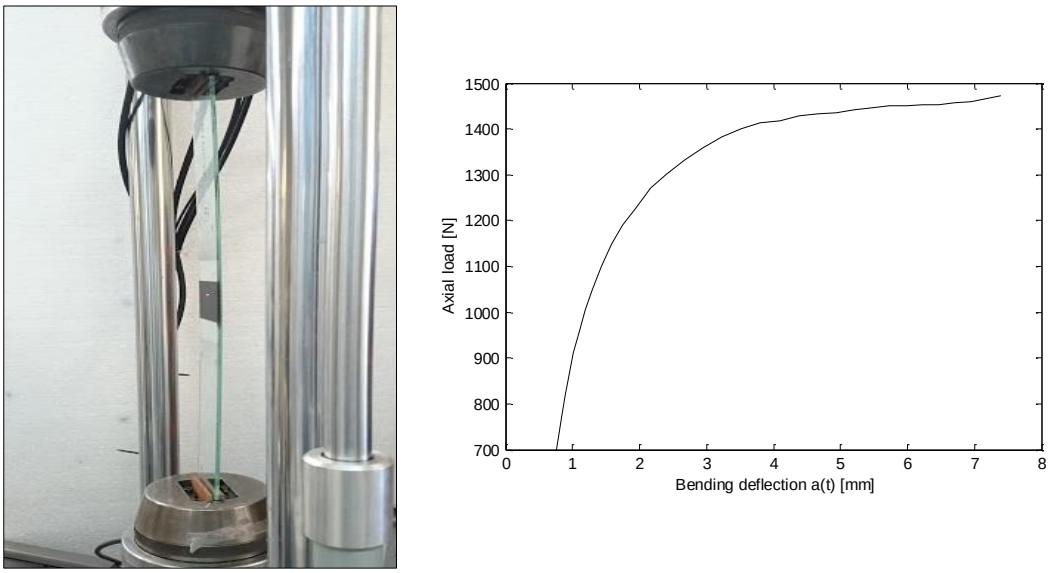

Figure 5. Buckling of pinned supported beam (L=700 mm, $H_1 = H_3 = 2.9\, mm, H_2 = 0.38\, mm$). Test setup (left) and axial load versus bending deflection at the mid-point of the beam.

In the analytical predictions a Young modulus $E_1 = 72$ GPa and Poisson ratio $\nu = 0.22$ were considered for the glass layers. With respect to the PVB, its mechanical properties have been determined in a previous work [10] by dynamic characterization in a DMA RSA3. A constant bulk modulus of $K_2(t) = 2\, GPa$ and the shear relaxation modulus

$G_2(t)$ presented in figure 2 corresponding to a reference temperature $T_0 = 20^oC$ were considered in the analytical predictions. Moreover, the effect of temperature was considered using the William, Landel and Ferry (WLF) model [26] where the TTS shift factor, a_T, is given by:

$$log(a_T) = -C_1 \frac{(T - T_0)}{C_2 + (T - T_0)} \tag{43}$$

where $C_1 = 12.60$ and $C2 = 74.46$ at $T_0 = 20^oC$.

The critical load predicted with Eq. (32) is presented in figure 6, which shows that, as expected, the critical load P_{crit} decreases with time. This means that the critical load N_{crit} [intersection of P_{crit} and (t)] will depend on the load history $P(t)$. The monolithic, layered, P^0_{crit} and P^∞_{crit} limits are also indicated in figure 6.

Figure 6 (right) also shows the analytical critical load P_{crit} predicted with Eq. (32) together with the experimental axial load acting on the beam. Buckling occurs when the curves corresponding to $P_{crit}(t, T)$ and to axial load $P(t)$ intersect. From figure 5, it is inferred that buckling should occur at $t = 672\ s$, from which it is determined that $N_{crit} = 1420\ N$. The maximum axial load reached in the test was $P_{max} = 1450\ N$. The discrepancy between P_{max} and N_{crit} was less than 2.5%. This agrees with [14], where it is demonstrated that due to the delay in the stress relaxation, a beam for which the viscoelasticity of the interlayer is fully considered appears to be stiffer than when the response is evaluated by means of the quasi-elastic approximation.

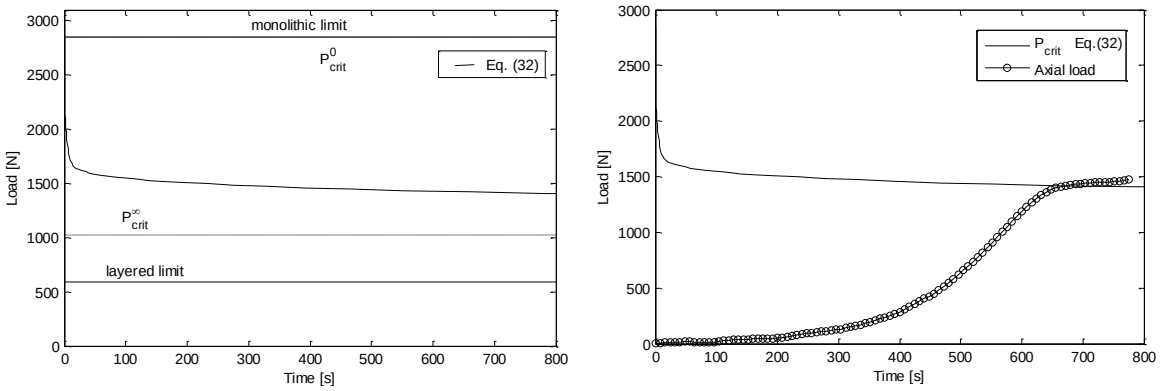

Figure 6. Buckling of a simply-supported beam ($L = 700\,mm, b = 0.1\,m, H_1 = H_3 = 2.9\,mm, H_2 = 0.38\,mm$): analytical prediction (left) and comparison between the experimental axial load and the predicted critical load (right).

As reflected in figure 6, for every axial-load time history acting on the beam, there is a critical time t_{crit} for which the instability is expected ($P(t) = P_{crit}(t, T)$). From Eq. (38), it can be inferred that this critical time depends on the load $P(t)$ but not on the initial imperfection e. Figure 7 presents the experimental bending deflection at the mid-point of beam versus time, together with the analytical deflection $a(t)$ predicted with Eq. (38) using the experimental axial load $P(t)$ shown in figure 6 and assuming initial imperfections $e =$ 0.1 mm and $e =$ 0.2 mm. The predicted critical time is $t_{crit} = 670$ s. The maximum bending deflection reached at the mid-point of the beam $a =$ 7 mm corresponds to a stress level of 25-30 MPa, which is close to the ultimate tensile stress of floated glass proposed in the codes [27].

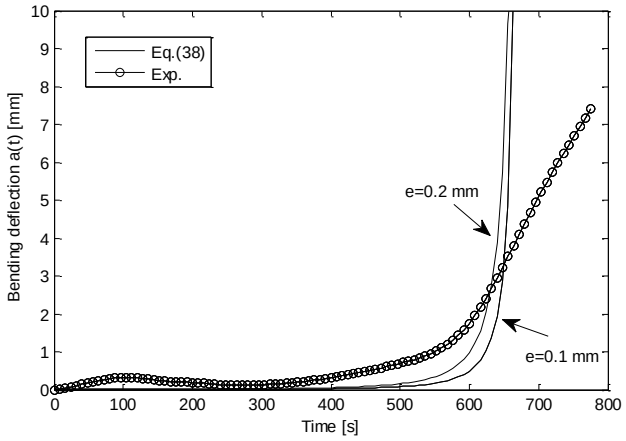

Figure 7. Experimental and analytical bending deflection at the mid-point of the beam. ($L = 700\,mm, b = 0.1\,m, H_1 = H_3 = 2.9\,mm, H_2 = 0.38\,mm$).

The same beam was tested for 4700 s applying the compressive load shown in Figure 8, where the maximum load level was 1300 N. The predicted critical time for this load was $t_{crit} =$ 7400 s, meaning that buckling should not occur during the test. Buckling was not detected during the experimental test, confirming the prediction.

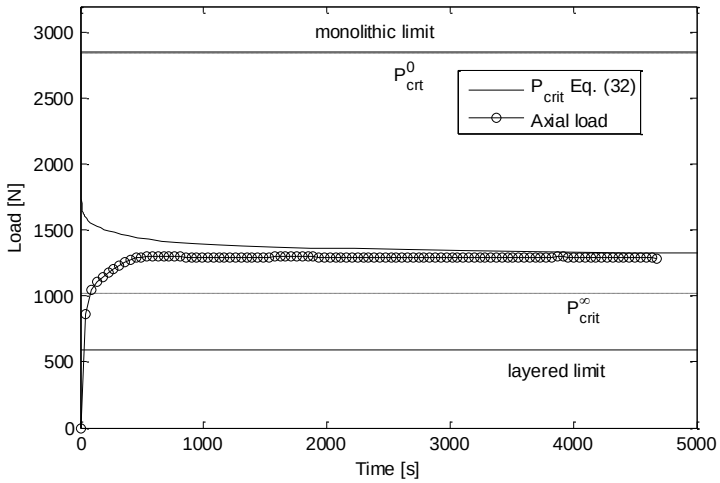

Figure 8. Buckling of simply supported beam ($L = 700\,mm, b = 0.1\,m, H_1 = H_3 = 2.9\,mm, H_2 = 0.38\,mm$) under compressive force (maximum force: 1.3 kN).

Figure 9 shows that the experimental bending deflection increases with time, the maximum deflection being 4.8 mm, this reaffirming that Eqs. (32) and (38) quite accurately predict the buckling of the beam. The deflection predicted with Eq. (33), assuming initial imperfections $e = 0.1$ mm and $e = 0.2$ mm, are also plotted in figure 9.

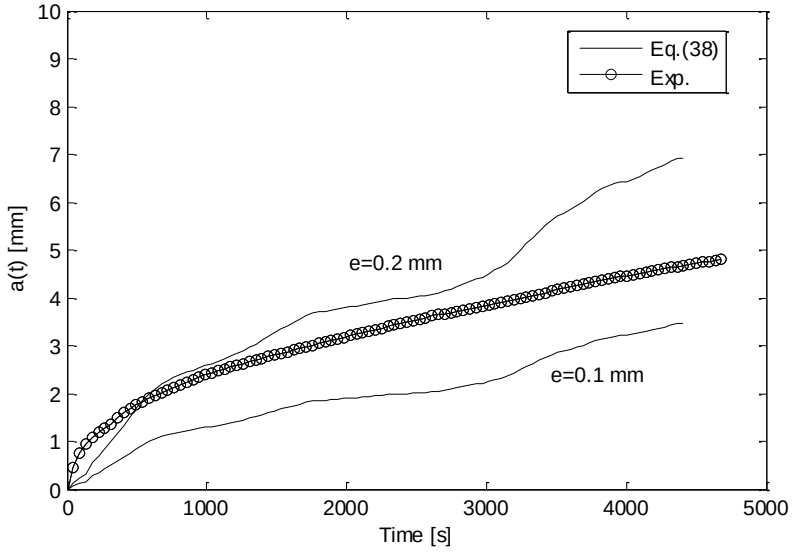

Figure 9. Experimental and analytical bending deflection at the mid-point of the beam under compressive force. ($L = 700\ mm,\ b = 0.1\ m, H_1 = H_3 = 2.9\ mm, H_2 = 0.38\ mm$).

Similar tests were performed in a shorter simply supported beam with $L = 0.5$ m and same thicknesses and width, i.e. $H_1 = 2.9$ mm, $H_3 = 2.9$ mm, $H_2 = 0.38$ mm, $b = 0.1$ m. The test was stopped when the bending deflection reached the magnitude of approximately 3.75 mm.

Figure 10 presents the analytical critical load predicted with Eq. (32) together with the experimental axial load acting on the beam (corresponding to a constant axial displacement rate of 0.01 mm/min). From the figure, we infer that buckling should occur at $t = 104\ s$, from which get $N_{crit} = 2360\ N$. The maximum axial load reached in the test was $P_{max} = 2420\ N$. The discrepancy between P_{max} and N_{crit} is less than 2.5%.

The experimental bending deflection at the mid-point of beam versus time is presented in figure 10 (right), together with the analytical deflections predicted with Eq. (38) using the experimental axial load $P(t)$ shown in figure 10 and assuming initial imperfections $e =$ 0.1 mm and $e =$ 0.2 mm. The predicted critical time is $t_{crit} = 115$ s. The maximum bending deflection reached at the mid-point of the beam $a =$ 3.75 mm corresponds to a stress level of 25-30 MPa, which is close to the ultimate tensile stress of floated glass proposed in the codes [27]

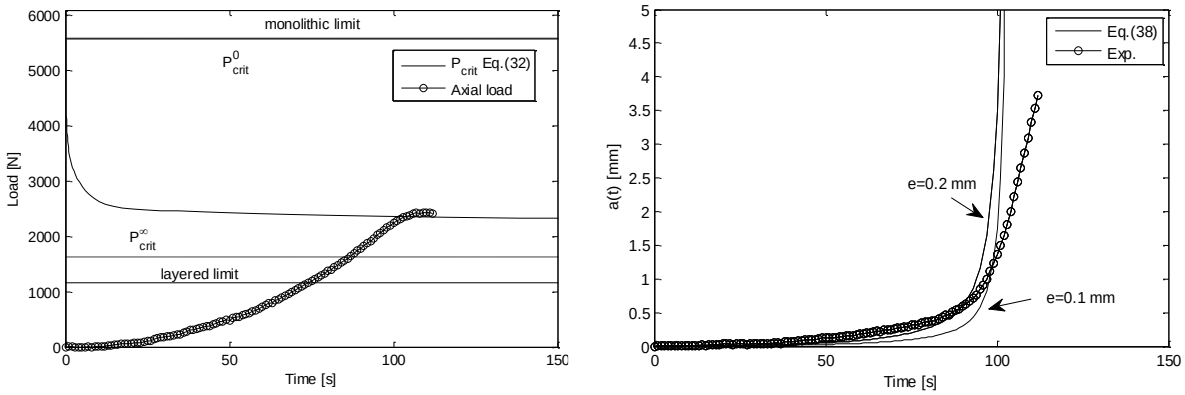

Figure 10. Buckling of simply supported beam ($L = 500\,mm, b = 0.1\,m, H_1 = H_3 = 2.9\,mm, H_2 = 0.38\,mm$), under constant axial displacement at rate 0.01 mm/min. Predicted critical load and experimental axial load (left). Predicted and experimental bending deflection at the mid-point of the beam (right).

The same beam was tested for 1480 s, applying the compressive load shown in figure 11, where the maximum load level is 2100 N. The specimen broke at $t = 1480\,s$ with a bending deflection of 9.4 mm. The predicted critical time is $t_{crit} =$ 1550 s. Figure 11 presents the experimental bending deflection together with that predicted with Eq. (38), assuming initial imperfections $e = 0.1\,mm$ and $e = 0.2\,mm$. The results presented in

figure 11 confirm that Eqs. (32) and (38) quite accurately predict the buckling of the beam.

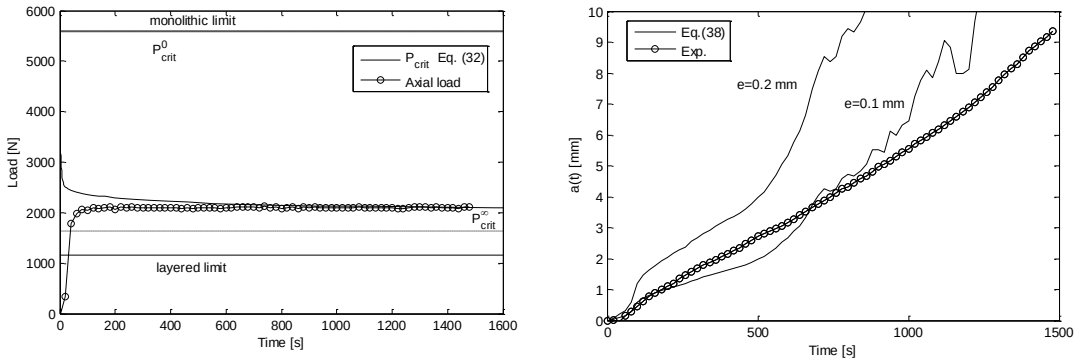

Figure 11. Buckling of simply supported beam ($L = 500\,mm, b = 0.1\,m, H_1 = H_3 = 2.9\,mm, H_2 = 0.38\,mm$) under compressive force (maximum force: 2.1 kN). Predicted critical load and experimental axial load (left). Predicted and experimental bending deflection at the mid-point of the beam (right).

3.2 Numerical simulations

Due to the brittleness of glass, fixed boundary conditions are difficult to reproduce in experimental tests. For the validation of Eq. (32) to any kind of boundary conditions, a finite-element model was assembled in ABAQUS [28] and the buckling load was predicted for simply supported, fixed-pinned and fixed-fixed boundary conditions. An ideal (no initial imperfections were considered) linear elastic planar model was assembled using quadrilateral linear plane-stress elements with the following geometrical data: $H_1 =$ 4 mm, $H_3 = 4$ mm, $H_2 = 0.38$ mm, $L = 1$ m, and $b = 0.1$ m. The mesh of the FE model together with some details of the boundary conditions are shown in figure 12.

The same material properties as those considered in Section 3 were considered for the glass layers. Because the model is linear elastic, the PVB interlayer was also modeled as

linear elastic. For each time $t = t_i$, the constant shear modulus $G_2 = G_2(t_i, T)$ and Poisson ratio $\nu_2 = 0.49$ were considered for the interlayer. A constant axial loading P was applied to the top of the model uniformly distributed. Then a standard linear elastic analysis was made to determine the stresses needed to form the geometric stiffness matrix K_G. Finally an eigenvalue buckling analysis was run to predict the critical load $P_{crit}(t_i, T)$ corresponding to each point of time $t = t_i$, which was calculated by:

$$P_{crit}(t_i, T) = \lambda_{1i} \cdot P \tag{43}$$

where λ_{1i} is the first eigenvalue or multiplier of the reference load P. The eigenvalue problem was solved using the Lanczos method [29].

The methodology is schematically shown in figure 13. This procedure was repeated for all the time points considered in the simulations.

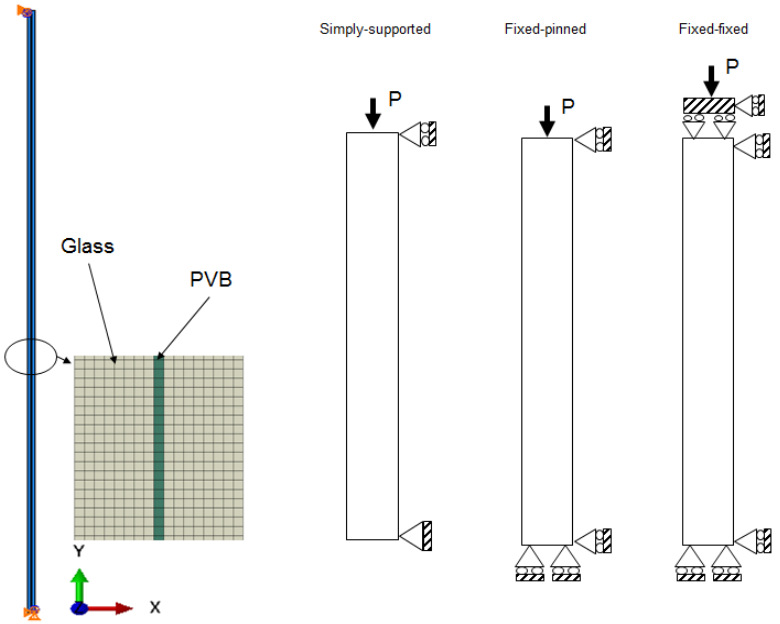

Figure 12. Model and mesh details of the numerical model used in the simulations.

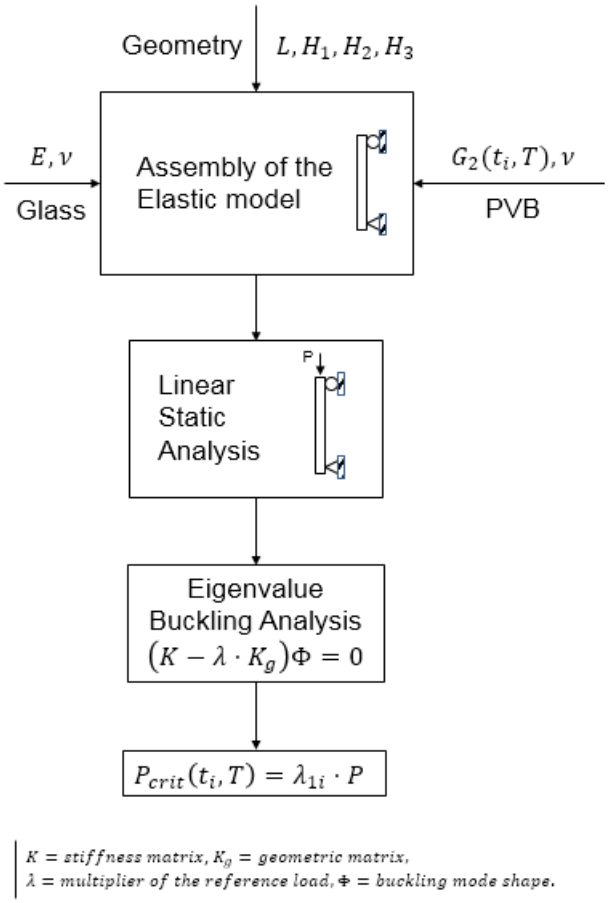

Figure 13. Methodology to calculate the critical load $P_{crit}(t_i, T)$ at time $t = t_i$.

Figure 14 presents the critical load predicted with Eq. (32) at $T = 20^o C$ and $T = 40^o C$ using the buckling ratio $\beta = 1$, together with the critical load obtained with the FE model. From the figure, it is inferred that the discrepancies between the numerical simulations and the analytical prediction with Eq. (32) are less than 0.15% for the simply supported boundary conditions.

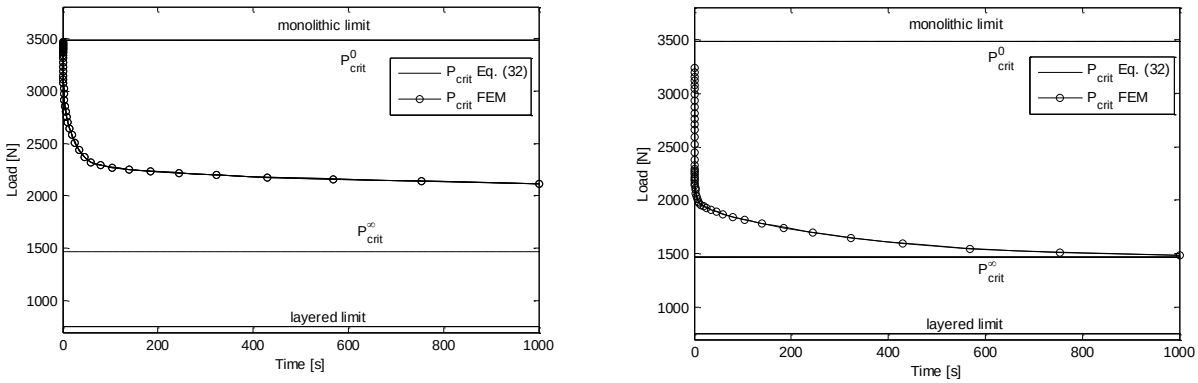

Figure 14. Analytical (Eq. (32)) and numerical critical loadings predicted for the simply supported beam: $T = 20^oC$ (left) and $T = 40^oC$ (right).

Figure 15 shows the analytical and the numerical critical loads predicted for the beam with fixed-pinned configuration at $T = 20^oC$ (left) and $T = 40^oC$ (right), respectively. In Eq. (32) the buckling ratio $\beta = 0.7$ was used. The discrepancies between the two models are less than 2.5%.

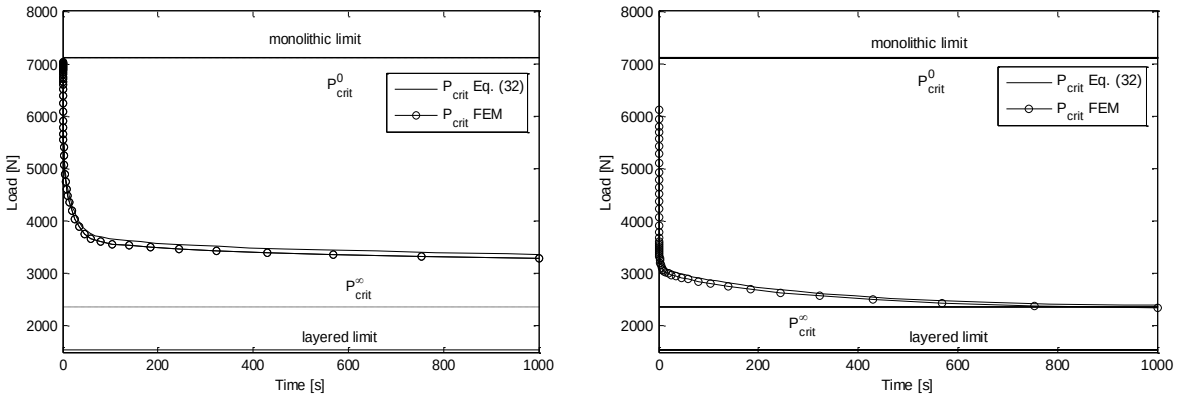

Figure 15. Analytical [Eq. (32)] and numerical critical loadings predicted for the fixed-pinned beam: $T = 20^oC$ (left) and $T = 40^oC$ (right).

Finally, the critical load of the fixed-fixed configuration was predicted with Eq. (32) using the buckling ratio $\beta = 0.5$. The analytical and the numerical predictions are shown in figure 15, from which it was found that discrepancies were less than 4.75%.

The results shown in figures 14 to 16 prove that Eq. (32) quite accurately predicts the buckling load of a laminated-glass beam with all the boundary conditions considered in the investigation.

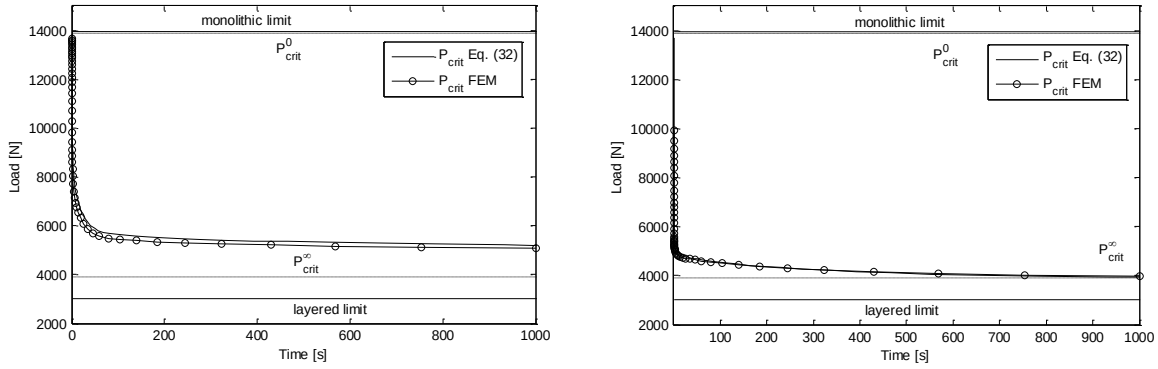

Figure 16. Analytical (Eq. (28)) and numerical critical loadings predicted for the fixed-fixed beam: $T = 20^oC$ (left) and $T = 40^oC$ (right).

4 CONCLUSIONS

Laminated-glass elements are slender and brittle and therefore structural stability is a design criterion to be considered when these elements are subject to compressive loads. Due to the viscoelastic behaviour of the interlayer materials, the critical load of a laminated-glass beam is time and temperature dependent. However, to avoid failures due to buckling, a safe procedure is needed and the compressive load acting on the beam must be less than the critical load P^{∞}_{crit} given by the long-term limit of the interlayer shear modulus G_2^{∞}. This also means that the quasi-elastic solution [5, 6, 8, 9] can be used advantageously to obtain safe critical loads in laminated glass, avoiding the use of numerical models or complicated analytical models.

In recent years, several analytical models have been proposed for determining the critical load of simply supported laminated-glass beams [12, 14, 15] using the effective stiffness and the effective thickness concepts. In this paper it is demonstrated that the effective stiffness is also dependent on the boundary conditions and its effect can be considered by means of the buckling ratios β used in the Euler theory with isotropic linear monolithic beams.

In this paper, a simple equation (Eq. 32) to calculate the buckling load of a laminated-glass beam subject to compressive load is proposed. This equation has been derived by extending the classical Euler theory for buckling of isotropic monolithic beams to laminated glass beams using the effective-stiffness and the effective Young modulus concept. The equation is easy to use, it can be applied to any kind of boundary conditions, and the buckling ratios of the classical Euler Theory for isotropic monolithic beams can be used in laminated-glass beams.

The accuracy provided by Eq. (32) has been validated by experimental compressive tests carried out on two simply supported beams 0.5 m and 0.7 m long, respectively, both of them with the following geometrical data: width $b = 0.1$ m, thickness of glass layers $H_1 = H_3 = 2.9$ mm and thickness of PVB layer $H_2 = 0.38$ mm. The tests were performed at room temperature $T = 24^oC$. The error between the experimental critical load and those predicted with Eq. (32) were consistently less than 3%.

Due to the brittleness of the glass, fixed boundary conditions are difficult to reproduce in monolithic and laminated-glass panels. For breakage prevention, contact between the glass and any other substance with a hardness equivalent to or greater than the hardness of glass should be avoided. Neoprene gaskets or other glazing materials are commonly used with frame systems. In order to validate Eq. (32) to fixed boundary conditions, a finite element model was assembled in ABAQUS [28] using quadrilateral linear plane stress elements and the critical load at temperatures $T = 20^oC$ and 40^oC was calculated. Simply supported, fixed-pinned, and fixed-fixed boundary conditions were considered in the simulations using the following geometrical data: length L= 1 m, width $b = 0.1$ glass thickness $H_1 = H_3 = 4$ mm, and PVB thickness $H_2 = 0.38$ mm. The discrepancies between the numerical and the analytical results (Eq. (32)) are less than 4.75% for all the boundary conditions considered in the simulations, demonstrating that Eq. (32) quite accurately predicts the buckling load of a laminated-glass beam with all the boundary conditions considered in this investigation.

ACKNOWLEDGEMENTS

The financing support given by the Spanish Ministry of Economy and Competitiveness through the project BIA2014-53774-R is gratefully appreciated.

REFERENCES

[1] Benninson, S., M.HX, Q. and Davies, P., High-performance laminated glass for structurally efficient glazing. Innovative Light-weight Structures and Sustainable Facades, Hong Kong, May, 2008.

[2] Zienkiewicz, O.C., Taylor, R.L. and Zhu, J.Z. The finite element method, its basis & fundamentals. 6th Edition. Elsevier.

[3] Foraboschi, P., Analytical model for laminated-glass plate, Compos Part B-Eng, 2012;43(5):2094-2106.

[4] Foraboschi, P., Three-layered plate: Elasticity solution. Compos Part B-Eng, in press, 2014.

[5] Foraboschi, P., Hybrid Laminated-Glass plate: Design and assessment. Compos Struct, 2013; 106:250-263.

[6] Galuppi, L., and Royer-Carfagni, G.F., The design of laminated glass under time-dependent load, Int J Mech Sci, 2012; 68:67-75.

[7] Calderone, I., Davies, P.S., and Benninson, S.J., Effective Laminate Thickness for the Design of Laminated Glass. *In: Glass Performance Days*, Tampere, Finland, 2009.

[8] Galuppi, L., and Royer-Carfagni, G.F., Laminated beams with viscoelastic interlayer, Int J Solids Struct. 2012;49:2637-2645.

[9] Galuppi, L., and Royer-Carfagni, G.F., Effective Thickness of Laminated Glass Beams: New Expression via a Variational Approach, J Eng Struct, 2012;38:53-67.

[10] López-Aenlle, M., Pelayo, F., Frequency Response of Laminated Glass Elements: Analytical Modelling and Effective Thickness, Appl Mech Rev, 2013;65(2), 020802 (13 pages).

[11] López-Aenlle, M., Pelayo, Dynamic effective thickness in laminated-glass beams and plates. Compos Part B-Eng. 2014; 67:332-347.

[12] Blaauwendraad, J., Buckling of laminated glass columns. HERON, 2007;52(1/2):147-218.

[13] Sattler, K., Stein, P., Ingenieurbauten 3, Theorie und Praxis, Springer-Verlag, Wien. 1974.

[14] Galuppi, L., and Royer-Carfagni, G.F., Buckling of three-layered composite beams with viscoelastic interaction. Compos Struct, 2014;107:512-521.

[15] Feldmann, M., Kasper, R. et al. Guidance for European Structural Desing of Glass Components. JCR Scientific and Policy Report, doi: 10.2788/5523, 2014.

[16] Foraboschi P. Buckling of a laminated glass column under test. Struct Eng, 2009;87(1).

[17] Timoshenko, S.P., Gere, J.M. Theory of elastic stability. McGraw Hill, London, 1963.

[18] Wölfel, E., Nachgiebiger Verbund Eine Näherungslösung und deren Anwendungsmöglichkeiten, In: Stahlbau, 1987;6:173-180.

[19] Foraboschi, P., Laminated glass column, Int J Struct Eng, 2009;87:20-26.

[20] Aiello S, Campione G, Minafò G, Scibilia N. Compressive behaviour of laminated structural glass members. Eng Struct 2011;33:3402–8.

[21] Amadio, C., Bedon, C., Analytical approaches for buckling verification of in-plane loaded laminated glass columns and panels. Architectural and Structural Applications of Glass. IOS Press, 2012.

[22] Norville, H.S., King, K.W., and Swoord, J.L., Behavior and strength of laminated glass," J Eng Mech. 1998;124(1):46-53.

[23] Ferry, J.D., Viscoelastic Properties of Polymers, Third ed., John Wiley & Sons, Ltd., New York. 1980.

[24] Tschoegl, N.W., The Phenomenological Theory of Linear Viscoelastic Behavior, Springer-Verlag, Berlin. 1989.

[25] Chajes, A., Principles of Structural Stability Theory (Civil engineering and engineering mechanics series). Prentice Hall, 1974.

[26] Williams, M.L., Landel, R.F., and Ferry, J., The Temperature Dependence of Relaxation Mechanisms in Amorphous Polymers and Other Glass-forming Liquids, J Am Chem Soc, 1955;77:3701-3707.

[27] PR EN.13474-1. Design of glass panes – Part 1: General basis for design. 2005.

[28] ABAQUS, Abaqus Theory Manual, Dessault Systemes, 2012.

[29] Petyt, M., Introduction to finile element vibration analysis, Cambridge University Press. 1990.

Figure Captions:

Figure 1. Schematic representation of a simply supported beam with an initial deformation.

Figure 2. Shear-relaxation modulus for the PVB at $T = 20^{o}C$ [10].

Figure 3. Effective stiffness of a simply supported beam with different lengths at $T = 20^{o}C$.

Figure 4. Buckling of a laminated-glass beam using the quasi-elastic approximation a) non-constant axial load P1(t); b) constant axial load P2(t); c) bending deflection a(t) for both loads, P1(t) and P2(t).

Figure 5. Buckling of pinned supported beam (L=700 mm, $H_1 = H_3 = 2.9\,mm, H_2 = 0.38\,mm$). Test setup (left) and axial load versus bending deflection at the mid-point of the beam.

Figure 6. Buckling of a simply-supported beam ($L = 700\,mm, b = 0.1\,m, H_1 = H_3 = 2.9\,mm, H_2 = 0.38\,mm$): analytical prediction (left) and comparison between the experimental axial load and the predicted critical load (right).

Figure 7. Experimental and analytical bending deflection at the mid-point of the beam. ($L = 700\,mm, b = 0.1\,m, H_1 = H_3 = 2.9\,mm, H_2 = 0.38\,mm$).

Figure 8. Buckling of simply supported beam ($L = 700\,mm, b = 0.1\,m, H_1 = H_3 = 2.9\,mm, H_2 = 0.38\,mm$) under compressive force (maximum force: 1.3 kN).

Figure 9. Experimental and analytical bending deflection at the mid-point of the beam under compressive force. ($L = 700\,mm,\ b = 0.1\,m, H_1 = H_3 = 2.9\,mm, H_2 = 0.38\,mm$).

Figure 10. Buckling of simply supported beam ($L = 500\,mm, b = 0.1\,m, H_1 = H_3 = 2.9\,mm, H_2 = 0.38\,mm$), under constant axial displacement at rate 0.01 mm/min.

Predicted critical load and experimental axial load (left). Predicted and experimental bending deflection at the mid-point of the beam (right).

Figure 11. Buckling of simply supported beam ($L = 500\,mm, b = 0.1\,m, H_1 = H_3 = 2.9\,mm, H_2 = 0.38\,mm$) under compressive force (maximum force: 2.1 kN). Predicted critical load and experimental axial load (left). Predicted and experimental bending deflection at the mid-point of the beam (right).

Figure 12. Model and mesh details of the numerical model used in the simulations.

Figure 13. Methodology to calculate the critical load $P_{crit}(t_i, T)$ at time $t = t_i$.

Figure 14. Analytical (Eq. (32)) and numerical critical loadings predicted for the simply supported beam: $T = 20^o C$ (left) and $T = 40^o C$ (right).

Figure 15. Analytical [Eq. (32)] and numerical critical loadings predicted for the fixed-pinned beam: $T = 20^o C$ (left) and $T = 40^o C$ (right).

Figure 16. Analytical (Eq. (28)) and numerical critical loadings predicted for the fixed-fixed beam: $T = 20^o C$ (left) and $T = 40^o C$ (right).